

# **Effect of torso morphology on maximum hydrodynamic resistance in front crawl swimming**

Christopher Papic <sup>a\*</sup>, Carla McCabe<sup>b</sup>, Tomohiro Gonjo<sup>c</sup> and Ross Sanders<sup>a</sup>

<sup>a</sup> *Exercise and Sport Science, Faculty of Medicine and Health, The University of Sydney, Sydney, Australia*

<sup>b</sup> *School of Sport, Faculty of Life and Health Sciences, Ulster University, Jordanstown, Northern Ireland*

<sup>c</sup> *Department of Physical Performance, Norwegian School of Sport Sciences, Oslo, Norway*

\*corresponding author

**Mailing address:** U3 69 Beaconsfield Street, Newport, 2106 (NSW, Australia)

**P:** +61 421 519 172

**E:** [chris.papic@sydney.edu.au](mailto:chris.papic@sydney.edu.au)

**Twitter:** @chris\_papic

# 1 **Effect of torso morphology on maximum hydrodynamic resistance in**

## 2 **front crawl swimming**

3 The aim of this study was to determine the influence of torso morphology on  
4 maximum instantaneous hydrodynamic resistance in front crawl swimming.  
5 Outlines of the torso in the frontal and anteroposterior planes were calculated from  
6 photographic images to determine continuous form gradients (m/m) for the  
7 anterior, posterior and lateral aspects of the torso. Torso cross-sectional areas at  
8 each vertical sample (0.001m) were used to calculate maximal rate of change in  
9 cross-sectional area ( $m^2/m^1$ ) in the chest-waist and waist-hip segments. During  
10 catch-up arm coordination in middle-long distance front crawl swimming, kicking  
11 propulsion is negligible and therefore the net force is equal to the drag during the  
12 non-propulsive hand phase. Drag coefficients were calculated at the instant of  
13 maximum horizontal deceleration of centre of mass during the non-propulsive  
14 hand phase of 400m pace front crawl stroke cycles. Maximal rate of change in  
15 cross-sectional area ( $r=0.44$ ,  $p=0.014$ ) and posterior form gradient ( $r=0.50$ ,  
16  $p=0.006$ ) of the waist-hip torso segment had moderate positive correlations with  
17 the coefficient of drag. A regression model including these two variables explained  
18 41% of the variance ( $p=0.001$ ). Indentation at the waist and curvature of the  
19 buttocks may result in greater drag force and influence swimming performance.

20 **Keywords:** anthropometry, drag coefficient, fluid dynamics, swimming  
21 performance

## 22 **Introduction**

23 The velocity of a human swimmer is determined by the interaction between propulsion  
24 developed actively by muscular contractions and resistive forces (hydrodynamic  
25 resistance) associated with movement of the body through water (Benjanuvatra,  
26 Blanksby, & Elliott, 2001; Pendergast et al., 2005). Understanding the relationship  
27 between body morphology and hydrodynamic resistance is important to identify  
28 differences in natural attributes of swimmers that affect their potential to succeed at a  
29 high level. Quantifying hydrodynamic resistance encountered by a swimmer is an  
30 ongoing challenge for researchers. Active drag, that is, the hydrodynamic resistance while  
31 swimming with stroking and kicking actions, has been estimated by various methods  
32 including the Measurement of Active Drag (MAD) system (Hollander et al., 1986). The  
33 MAD system is based on the assumption that at constant average velocity across stroke  
34 cycles the net impulse for a single stroke cycle is zero and therefore the propulsive and  
35 hydrodynamic resistive impulses are equal in magnitude (Van der Vaart et al., 1987).  
36 However, swimmers' velocities fluctuate throughout the front crawl stroke cycle due to  
37 the various propulsive and recovery phases (Alcock & Mason, 2007; Psycharakis, Naemi,  
38 Connaboy, McCabe, & Sanders, 2010) making it difficult to quantify the actual  
39 instantaneous drag forces to assess the effect of body shape characteristics on  
40 hydrodynamic resistance.

41 Hydrodynamic resistance brought about by the arms during the front crawl stroke  
42 cycle is the lowest in magnitude during the non-propulsive hand phase, with one arm  
43 outstretched in front of the swimmer preparing for the 'catch' and the other arm above  
44 the water surface (Gatta, Cortesi, Fantozzi, & Zamparo, 2015). This arm coordination is  
45 known as 'catch-up' and is commonly exhibited by swimmers during middle- and long-  
46 distance front crawl swimming (Seifert, Chollet, & Bardy, 2004). Assuming that the  
47 propulsive force due to the kick is negligible, the net force during this period of the stroke

48 cycle is affected only by hydrodynamic resistance. Consequently, the magnitude of  
49 deceleration of the swimmer during the non-propulsive hand phase provides an  
50 opportunity to assess the effects of the swimmer's morphology on hydrodynamic  
51 resistance.

52         With respect to human swimming, fluid flow may separate from the boundary  
53 layer, the layer of fluid flow in contact with the body, due to the morphology of the  
54 swimmer (Mollendorf, Albert, Oppenheim, & Pendergast, 2004). This separation from  
55 the boundary layer creates turbulent flow and a resulting pressure differential causing  
56 increased form drag (Marinho, Barbosa, Rouboa, & Silva, 2011), the drag produced from  
57 the physical characteristics of the body (Hertel, 1966). Marine animals exhibit body shape  
58 characteristics that minimise hydrodynamic resistance. One characteristic that aids  
59 dolphins in minimising form drag is a low rate of change in cross-sectional area (CSA)  
60 when progressing caudally (Fish & Hui, 1991). Furthermore, the form gradient, the rate  
61 of change in the body outline in the frontal and anteroposterior planes, is gradual without  
62 sudden changes in curvature. A low rate of change in CSA and a low form gradient  
63 minimises turbulence and disruption to fluid flow around the body than a high rate of  
64 change. Morphological characteristics that minimise turbulence along a body are  
65 advantageous for reducing hydrodynamic resistance. There is an assumption that areas of  
66 the human torso such as the indentation of the waist and curvature of the buttocks may  
67 have rapid changes in curvature when compared with dolphins, which may disrupt fluid  
68 flow around the body when moving through the water.

69         Analysis of the effects of torso morphology on hydrodynamic resistance and  
70 performance has focused predominantly on singular anthropometric measures; breadths,  
71 circumferences and CSA (Benjanuvatra et al., 2001; Lyttle, Blanksby, Elliot, & Lloyd,  
72 1998). In relation to swimming humans, 'projected frontal area' or 'trunk transverse

73 surface area' (TTSA) refers to the largest CSA of the swimmer in the transverse plane of  
74 the body. TTSA has been calculated using the planimetric method from 2D digital images  
75 in the transverse plane taken above the swimmer whilst on land (Morais et al., 2011;  
76 Vilas-Boas et al., 2010) and from the frontal view of a swimmer during free-swimming  
77 and underwater mono-fin swimming (Gatta et al., 2015; Nicolas, Bideau, Colobert, &  
78 Berton, 2007). Male swimmers have been shown to have larger active drag and drag  
79 coefficient values than female swimmers during front crawl swimming without kicking  
80 actions, which has been attributed to a larger TTSA (Toussaint et al., 1988). TTSA in the  
81 transverse plane with two arms extended above the head was found to have a high positive  
82 correlation with the coefficient of drag during front crawl swimming without kicking  
83 actions ( $r=0.87$ ) (Huijing et al., 1988). TTSA considers additional body segments that  
84 protrude beyond the chest CSA in the transverse plane, such as the shoulders and hips,  
85 that can increase hydrodynamic resistance. While a relationship has been found between  
86 TTSA and hydrodynamic resistance in front crawl, TTSA represents a 2D image and  
87 therefore does not consider curvatures along the torso or the site in which curvatures and  
88 indentations reside that may influence hydrodynamic resistance. Mollendorf et al. (2004)  
89 proposed that significant changes in curvature along the body may result in fluid flow  
90 separation and the subsequent turbulence and pressure differentials.

91         While there is some evidence that morphological characteristics of the torso affect  
92 hydrodynamic resistance, singular measures do not consider the effect of shape variations  
93 along the length of the torso that influence fluid flow and hydrodynamic resistance. The  
94 aim of this study was to determine the influence of torso morphology on maximum  
95 instantaneous hydrodynamic resistance in front crawl swimming. It was hypothesised that  
96 the rate of change in CSA and form gradient when progressing caudally along the torso  
97 would be associated with hydrodynamic resistance during front crawl swimming.

98 Knowledge of morphological characteristics of the torso that minimise hydrodynamic  
99 resistance may be useful for identifying talent, manipulating swimming technique and for  
100 optimising body shape through strength and conditioning, swimming training, and  
101 nutritional strategies.

## 102 **Methods**

### 103 *Participants*

104 Photographic imaging and whole-body centre of mass data sets of male swimmers were  
105 used from studies conducted by McCabe and Sanders (2012) at the Centre for Aquatics  
106 Research and Education (CARE), The University of Edinburgh, and Gonjo et al. (2019)  
107 at the Aquatics Research Centre at the University of Porto. These were defined as Group  
108 1 and Group 2, respectively. These data sets were used as the methods of data collection  
109 and quantification of whole-body centre of mass were consistent. Group 1 included 15  
110 Scottish national and international level male swimmers; seven sprint specialists  
111 ( $18.3 \pm 2.3$  years,  $75.8 \pm 6.4$  kg,  $184.4 \pm 6.3$  cm, 400m front crawl swim time  
112  $4.24.2 \text{ mins} \pm 9.10 \text{ sec}$ , 50m front crawl swim time less than 24.60sec) and eight distance  
113 specialists ( $17.5 \pm 2.5$  years,  $72.3 \pm 10.5$  kg,  $181.8 \pm 7.5$  cm, 400m front crawl swim time  
114  $4.02.59 \text{ min} \pm 7.08 \text{ s}$ ) (McCabe & Sanders, 2012). Group 2 included ten male national level  
115 Portuguese swimmers ( $17.47 \pm 1.00$  years;  $70.05 \pm 6.63$  kg;  $179.14 \pm 5.43$  cm, 100m front  
116 crawl swim time  $54.50 \pm 1.23$  sec) (Gonjo et al., 2019). Despite differences in event  
117 speciality, no kinematic differences were found between the sprint and distance specialist  
118 swimmers at 400m front crawl swimming pace (McCabe & Sanders, 2012). Testing  
119 procedures were approved by the relevant institutional ethics committees and all  
120 swimmers provided written informed consent to participate in the study.

121 *Experimental design*

122 *Photographic imaging*

123 Photographic images of the swimmers were obtained for two purposes. The first was to  
124 enable body segment parameters to be determined by the Elliptical Zone Method for  
125 subsequent calculation of each participant's centre of mass position (Deffeyes & Sanders,  
126 2005). The second was to enable the contours of the torso to be traced for subsequent  
127 analysis of the effect of torso shape on the drag coefficient. Swimmers in Group 1 and  
128 Group 2 were marked with black circular marks (Grimas Crème Make Up) on nineteen  
129 anatomical landmarks for the calculation of centre of mass: the vertex of the head, the  
130 right and left of the: tip of the third distal phalanx of the finger, wrist axis, elbow axis,  
131 shoulder axis, hip axis, knee axis, ankle axis, fifth metatarsophalangeal joint, and the tip  
132 of the first phalanx (Deffeyes & Sanders, 2005). Two digital cameras, Nikon E4200  
133 (Minato, Tokyo, Japan) and Canon Ixus 400 (Ōta, Tokyo, Japan) were positioned on  
134 tripods at a height of 1.0m with their axis aligned horizontally and perpendicular to the  
135 swimmers' frontal and anteroposterior planes. The swimmers were photographed in the  
136 anatomical position wearing regular swimming trunks to facilitate valid comparison of  
137 body shape characteristics between swimmers. In both the anterior and lateral images, the  
138 swimmer's arms were positioned such that the outline of the torso was visible for tracing.

139 *Data collection and processing*

140 Swimmers completed an individual warm-up consisting of stretching, front crawl  
141 swimming and swimming drills. Swimmers in Group 1 performed a maximal evenly  
142 paced 400m front crawl swim through a 6.75m<sup>3</sup> calibrated space. Swimmers in Group 2  
143 performed a 50m front crawl swimming trial at 400m front crawl swimming velocity  
144 through a 30.0m<sup>3</sup> calibrated space. The swimmers were recorded by four above and two

145 below water JVC KY32 CCD (Long Beach, California, USA) cameras for Group 1 and  
146 HDR-CX160E (Tokyo, Japan) cameras for Group 2. The cameras were synchronised and  
147 recorded at 50Hz. A single stroke cycle was captured in the middle of the pool during  
148 each 50m segment of the 400m trial for swimmers in Group 1. To facilitate valid within-  
149 participant comparison in the current study, laps 1 and 6–8 were removed to negate the  
150 influence of greater swimming velocities in lap 1 than the remainder of the 400m trial  
151 and the fatigue effect in laps 6–8. Thus, a total of four captured stroke cycles were  
152 analysed per swimmer corresponding to laps 2–5. A single stroke cycle was captured in  
153 the middle of the pool during the 50m trial of swimmers in Group 2.

154 All swimmers were instructed to not breathe during the captured stroke cycle.  
155 This minimised possible confounding of drag coefficients by breathing technique and the  
156 associated lateral body movements, as lateral body movements are found to increase  
157 hydrodynamic resistance (Zamparo, Gatta, Pendergast, & Capelli, 2009). Nineteen  
158 anatomical landmarks on the participants were manually digitised, by the same operator,  
159 for each video frame using APAS (Ariel Dynamics Inc., San Diego, USA) for the above  
160 and below water fields of view prior to calculation of three-dimensional (3D) coordinates  
161 by the APAS direct linear transformation process. Digitising reliability was found to be  
162 acceptable with small reported errors in mean centre of mass velocity (m/s, SD=0.01,  
163 coefficient of variation=0.22) after digitising a single stroke cycle ten times by the same  
164 operator (McCabe, Psycharakis, & Sanders, 2011). The 3D coordinates and the body  
165 segment parameter data were then input to a bespoke MATLAB program (Mathworks  
166 Inc., Massachusetts, USA) to calculate centre of mass position. The centres of mass  
167 coordinates were interpolated using Fourier transform and inverse transform to 201 points  
168 (Group 1) representing half percentiles of the stroke cycle, and 101 points (Group 2)  
169 representing percentiles of the stroke cycle. A stroke cycle was defined as the instant of



170 entry of one hand to the instant of re-entry of the same hand. Instantaneous horizontal  
171 velocities ( $v$ , m/s) and accelerations ( $\alpha$ , m/s<sup>2</sup>) of centre of mass were derived for each  
172 sample ( $i$ ) of the  $x$  (swimming direction) coordinate of the centre of mass displacement  
173 ( $x$ , m) data using Equation 1 and Equation 2, respectively. Initial coordinate data filtering  
174 (4<sup>th</sup> Order Butterworth with a cut off frequency of 6Hz) ensured that the minimum and  
175 maximum velocity and acceleration peaks identified from the derived time series were  
176 not inflated by noise.

$$177 \quad v(i) = \frac{x(i+1) - x(i-1)}{t(i+1) - t(i-1)} \quad (1)$$

$$178 \quad \alpha(i) = \frac{x(i+1) - 2x(i) + x(i-1)}{[t(i+1) - t(i)]^2} \quad (2)$$

### 179 ***Torso shape analysis***

180 The photographic images were input into the bespoke MATLAB program ‘TorsoShape’  
181 adapted from the ‘eZone’ program (Deffeyes & Sanders, 2005) as described by Papic et  
182 al. (2019). Calibration for the front and side views involved digitising images of the  
183 calibration frame for five control markers in the X-axis spaced 0.2m apart and six control  
184 markers in the Y-axis spaced 0.2m apart. A single operator then traced, using a mouse  
185 and cursor, the outlines of the torso from the front and side views. The tracings extended  
186 beyond the C7 and greater trochanter landmarks to eliminate endpoint distortion in  
187 subsequent low-pass filtering. A zoom function ensured accuracy during the calibration  
188 and tracing of the swimmer’s torso. The program interpolates the sampled points to yield  
189 the two-dimensional coordinates of the tracings with the vertical (Z) coordinates being  
190 1mm apart, smooths the data at 12Hz using a Butterworth 4<sup>th</sup> order digital filter and aligns  
191 the 1mm samples of the four tracings to a common vertical reference. The program  
192 automatically outputs the coordinates of each tracing for the frontal plane (X, Z) and for  
193 the anteroposterior plane (Y, Z) and the difference between the X coordinates at each Z  
194 sample and the Y coordinates at each Z sample.

195 *Cross-sectional area*

196 The torso was modelled as a series of vertically stacked ellipses (Jensen, 1978) at 1 mm  
197 increments using the differences in X and Y coordinates as the diameters of each ellipse.  
198 Transverse and anteroposterior diameters are initially converted to radii (a and b,  
199 respectively). The area of an ellipse formula ( $CSA = \pi ab$ ) was used to estimate CSAs  
200 moving caudally along the torso. The largest CSA between C7 vertebrae height and the  
201 waist was defined as ‘chest CSA’ ( $m^2$ ), the smallest CSA as ‘waist CSA’ and the CSA at  
202 the greater trochanter as ‘hip CSA’.

203 *Rate of change in cross-sectional area*

204 Previous research compared the maximal rate of change in CSA between a male and  
205 female mannequin (Pease & Vennell, 2011). Using Microsoft Excel (Microsoft Corp.,  
206 Washington, USA), the change of the CSA values between adjacent vertical increments  
207 (0.001m) were calculated using the central difference formula and represented the rate of  
208 change in CSA moving caudally along the swimmer’s torso. The greatest rate of change  
209 in CSA between chest-waist and waist-hip ( $m^2/m$ ) was calculated for each segment. A  
210 negative rate of change indicates that CSA is reducing when progressing caudally, whilst  
211 a positive value indicates that CSA is increasing.

212 *Form gradients*

213 Form gradients indicated the ‘suddenness’ of body shape change in the swimmer’s body  
214 outline in the frontal and anteroposterior planes. The maximum form gradient (m/m) of  
215 the left and right lateral aspects of the torso in the frontal plane (X, Z) and anterior and  
216 posterior aspects of the torso in the anteroposterior plane (Y, Z) were calculated in  
217 Microsoft Excel from the coordinate values of the swimmer’s torso outline using the first  
218 central difference formulae; Equation 3 and Equation 4, respectively. Each form gradient

219 was separated into chest-waist and waist-hip segments to assess change in curvature  
220 between the points at which the CSAs were maximum at the chest and hips and minimum  
221 at the waist (Figure 1). For the side and front camera views of the torso, a negative form  
222 gradient indicated that the portion of the torso was sloping inwards with respect to the  
223 longitudinal axis, whilst a positive form gradient indicated that the torso was sloping  
224 outwards with respect to the longitudinal axis.

225

$$226 \quad \text{FG}_{\text{Frontal}}(i) = \frac{X(i+1) - X(i-1)}{Z(i+1) - Z(i-1)} \quad (3)$$

$$227 \quad \text{FG}_{\text{Anteroposterior}}(i) = \frac{Y(i+1) - Y(i-1)}{Z(i+1) - Z(i-1)} \quad (4)$$

228

229 Figure 1. Maximum segment form gradient (m/m): Lateral (right) chest-waist (1–3) and  
230 waist-hip (3–5), lateral (left) chest-waist (2–4) and waist-hip (4–6), posterior chest-waist  
231 (7–9) and waist-hip (9–11), anterior chest-waist (8–10) and waist-hip (10–12).

### 232 ***Coefficient of drag***

233 The coefficient of drag is commonly used as an indicator of the influence of the shape  
234 characteristics of a body on hydrodynamic resistance. As such, it is useful to explain  
235 differences in swimming performance (Havriluk, 2005). The estimate of the coefficient  
236 of active drag can be obtained if the resistive force, water density, cross sectional area,  
237 and velocity are known. However, as is the case with the estimate of active drag it is  
238 generally based on the drag experienced during a whole stroke cycle or several stroke  
239 cycles and therefore represents a mean value despite periods of acceleration and  
240 deceleration in the stroke cycle. One of the few studies to obtain a coefficient  
241 corresponding to particular events involving deceleration of the swimmer was conducted  
242 by Vilas-Boas et al. (2010). They obtained a coefficient of drag during the first and second

243 gliding positions of the underwater breaststroke stroke following the dive or turn using  
244 deceleration force derived by inverse dynamics. Similarly, Morais et al. (2013) obtained  
245 coefficients of swimmers during underwater gliding in a static streamlined body position.  
246 While the net deceleration force in the breaststroke and streamlined gliding positions are  
247 equal to the resistive force, a conceptual approach similar to those studies can be applied  
248 to the catch-up portion of the front crawl stroke cycle where propulsive force from kicking  
249 is negligible.

250         The coefficient of drag force in the current study was determined by rearranging  
251 the equation embodying Newton's second law of motion to obtain the total drag force  
252 (Equation 5). The maximum coefficient of drag ( $C_d$ ), at the time swimmers did not  
253 perform propulsive upper-limb motion, was obtained from Equation 6 with values input  
254 for the swimmer's total mass ( $m$ ) (body mass and added fluid mass) (Morais et al., 2013),  
255 maximal CSA ( $A$ ), velocity ( $v$ ), acceleration ( $\alpha$ ) and fluid density ( $\rho$ ) (1000 kg/m<sup>3</sup>). Total  
256 mass was calculated as body mass (kg) multiplied by 1.268, as male swimmers have been  
257 found to have an average added mass of 26.8% (Caspersen, Berthelsen, Eik, Pâkozdi, &  
258 Kjendlie, 2010). Added mass is the mass of fluid moving in conjunction with the body,  
259 including the boundary layer (Naemi & Sanders, 2008). Previous research supports the  
260 use of maximal CSA to substitute for  $A$  and a power of two for swimming velocity  
261 (Havriluk, 2005). An instantaneous measure of maximum deceleration (m/s<sup>2</sup>) during the  
262 non-propulsive hand phase defined the acceleration term ( $\alpha$ ) of Equation 6. The drag  
263 coefficient derived for each of the four stroke cycles per swimmer in Group 1 were  
264 averaged to represent a mean drag coefficient for each swimmer.

265

$$266 \quad Fd = m \cdot \alpha = \frac{1}{2} \cdot Cd \cdot \rho \cdot A \cdot v^n \quad (5)$$

267 
$$Cd = \frac{(m \cdot \alpha \cdot 2)}{(\rho \cdot A \cdot v^2)} \quad (6)$$

268 ***Statistical analysis***

269 Statistical analysis was performed using SPSS software (Version 25, SPSS Inc., Chicago,  
270 USA). Independent sample Welch's T-tests were performed between Group 1 and Group  
271 2 for torso shape measurements and drag coefficients to determine whether differences  
272 existed between the two sample sets. If no differences existed between the groups, the  
273 groups would be combined to increase the sample size. Pearson correlation coefficients  
274 were calculated to determine the influence of each torso shape measure on the coefficient  
275 of drag. Pearson correlation coefficient strength of association was defined by the  
276 following criteria:  $r=0-0.19$  as very weak,  $r=0.2-0.39$  as weak,  $r=0.40-0.59$  as moderate,  
277  $r=0.60-0.79$  as strong and  $r=0.8-1.0$  as very strong (Evans, 1996). A stepwise linear  
278 regression analysis was conducted using the SPSS linear regression 'step-wise' function,  
279 to determine the relationship of torso shape measures and the coefficient of drag during  
280 front crawl swimming. The 'bootstrap' statistical function for linear regressions in SPSS  
281 was conducted with 2000 bootstrap sample iterations on significant predictors of the drag  
282 coefficient. Bootstrapping is a non-parametric data resampling technique that retrieves  
283 random samples from the total data set and estimates the indirect effects in each  
284 resampled data set (MacKinnon, Lockwood, & Williams, 2004). Bootstrapping is used to  
285 improve the accuracy of statistical estimations (Juan & Lantz, 2001). Bootstrapping was  
286 used to derive bias-corrected and accelerated 95% confidence intervals for Pearson  
287 correlation coefficients and the statistical significance of predictors in the regression  
288 model. Statistical significance was accepted at  $p<0.05$ .

289 **Results**

290 Mean torso shape measures and drag coefficient values for the two data sets (Group 1 and  
291 Group 2) and the combined cohort are reported in Table 1. There were no significant  
292 differences in torso morphology and coefficient of drag values between Group 1 and  
293 Group 2. Consequently, Group 1 and Group 2 were pooled together as a combined cohort  
294 of swimmers (n=25) to determine the influence of torso morphology on the coefficient of  
295 drag.

296

297 Table 1. Mean (standard deviation) torso shape and drag coefficient measurements for  
298 Group 1, Group 2 and Combined Cohort.

299

300 Significant moderate positive correlations were found between rate of change in CSA  
301 ( $r=0.44$ ,  $p=0.014$ ; 95% CI=0.16, 0.69) and the posterior form gradient waist-hip ( $r=0.50$ ,  
302  $p=0.006$ ; 95% CI=0.15, 0.74) with the drag coefficient. The two torso shape  
303 measurements and their relationship with the drag coefficient are independently  
304 expressed in Figure 2 and Figure 3 with their respective Pearson correlation coefficients.  
305 Table 2 summarises the Pearson correlation coefficients for all torso shape measurements  
306 and their influence on the drag coefficient. Using the stepwise regression method it was  
307 found that the rate of change in CSA waist-hip ( $\beta=0.46$ ,  $p=0.007$ ) and the posterior form  
308 gradient waist-hip ( $\beta=0.52$ ,  $p=0.003$ ) were significant predictors of the coefficient of drag  
309 during front crawl swimming, explaining 41% of the variance (*adjusted*  $R^2=0.41$ ,  
310  $p=0.001$ ). The linear regression bootstrapping procedure, with 2000 bootstrap resample  
311 iterations, revealed that the rate of change in CSA waist-hip ( $p=0.009$ ) and posterior form  
312 gradient waist-hip ( $p=0.001$ ) were still significant predictors of maximal drag coefficients  
313 in front crawl swimming.

314

315 Table 2. Pearson correlation coefficient between torso shape measurements and the drag  
316 coefficient (n=25).

317

318 Figure 2. Maximum rate of change in cross sectional area waist-hip vs maximum drag  
319 coefficient.

320

321 Figure 3. Maximum posterior form gradient waist-hip vs maximum drag coefficient.

## 322 **Discussion and implications**

323 This study quantified the rate of change in CSA and the form gradients of the anterior,  
324 posterior and lateral aspects of the torso to determine the relationship between torso  
325 morphology and an instantaneous drag coefficient during front crawl swimming. It was  
326 hypothesised that a relationship would exist between the rate of change in CSA and  
327 hydrodynamic resistance and form gradient of the torso and hydrodynamic resistance  
328 during front crawl swimming. In support of the hypothesis, maximum rate of change in  
329 CSA waist-hip and posterior form gradient waist-hip had moderate positive correlations  
330 with the drag coefficient, accounting for 41% of variance when combined in the  
331 regression equation. A high rate of change in CSA when progressing caudally from the  
332 waist and a greater posterior form gradient indicated a larger indentation at the waist and  
333 curvature of the buttocks, respectively.

334 While the causal mechanism of the relationship between rate of change in CSA  
335 and posterior form gradient on the coefficient of drag cannot be confirmed by the  
336 findings, previous research can give insight into the association between indentation at  
337 the waist and curvature of the hips with fluid flow. Pressure area analysis, using CFD, of  
338 a national level female swimmer's body was conducted during underwater gliding in the

339 streamlined horizontal body position (Beaumont, Taiar, & Polidori, 2017). It was found  
340 that the largest total pressure area (pascals) produced by fluid flow on the body was the  
341 head of the swimmer, whilst the arms, superior aspect of the buttocks and posterior  
342 aspects of the legs were the next significant pressure areas. The pressure area in the  
343 section from the lumbar region to the buttocks is of interest as it coincides with the  
344 posterior form gradient waist-hip segment analysed in the current study and supports  
345 Mollendorf et al. (2004) who hypothesised that fluid flow separation and the subsequent  
346 generation of turbulence and pressure differentials may occur along the body where there  
347 are significant changes in curvature. This implies that manipulating body positioning and  
348 stroke mechanics to minimise curvatures, such as excessive lordosis in the lower back  
349 region, may reduce hydrodynamic resistance.

350 In that vein, manipulation of torso morphology of one male international level  
351 swimmer has been achieved by wearing a whole-body swimsuit (Machtsiras, 2012). The  
352 use of a whole-body swimsuit had a significant effect on the glide factor, a measure of  
353 hydrodynamic efficiency of the body derived using the 'Hydro-Kinematic' method, of  
354 the male swimmer ( $d=3.317$ ,  $p<0.001$ ) (Naemi & Sanders, 2008). Improvements in the  
355 swimmer's glide factor by 16.7% when wearing the whole-body swimsuit were thought  
356 to be due to morphological changes to the swimmer's body (Machtsiras, 2012). These  
357 changes included a reduction in CSAs of the chest by 1.95% and the hips by 3.67%, whilst  
358 increasing the CSA of the waist by 8.21%, when comparing the whole-body swimsuit  
359 with the regular swimsuit (Machtsiras, 2012). Reducing chest and hip CSA, whilst  
360 increasing waist CSA would theoretically reduce the rate of change in CSA waist-hip and  
361 the posterior form gradient waist-hip of the swimmer. While whole-body swimsuits are  
362 currently banned in competitive swimming, their reduction in body CSAs and subsequent  
363 improvement in glide efficiency support the findings from the current study, whereby the



364 magnitude of curvature from waist-hip was associated with the hydrodynamic properties  
365 of the swimmer's body.

366 To our knowledge, this is the first study to quantify curvatures of the torso to  
367 assess their influence on hydrodynamic resistance. While Pease and Vennell (2011)  
368 investigated the rate of change in CSA of the body and referred to curvatures along the  
369 torsos of male and female mannequins, they did not calculate form gradients or an  
370 equivalent measure of the body outline. The advantage of calculating form gradients in  
371 the frontal and anteroposterior planes is that rate of change in CSA does not distinguish  
372 the shape characteristics or direction, with respect to the path of fluid flow, of body mass  
373 distribution along the torso. Swimmers of similar body mass and rate of change in CSA  
374 from waist-hip could have different form gradients representative of different curvatures  
375 produced by posture and body mass distribution around the lower abdomen, iliac crest or  
376 buttocks. For example, two swimmers from Group 1 had a body mass difference of 1.9%  
377 (74.8kg vs 76.2kg) and maximal rate of change in CSA waist-hip difference of 4.2%  
378 ( $0.268\text{m}^2/\text{m}$  vs  $0.279\text{m}^2/\text{m}$ ), but differed in their posterior form gradient waist-hip and  
379 drag coefficient values by 12.3 % ( $0.570\text{m}/\text{m}$  vs  $0.640\text{m}/\text{m}$ ) and 48.3% (2.40 and 3.56),  
380 respectively.

381 Instantaneous drag coefficients calculated in the current study from front crawl  
382 swimming were significantly greater than those derived from front crawl active drag  
383 analysis throughout the literature. The mean of drag coefficients derived in previous  
384 research from added and/or subtracted active drag methods, such as the velocity  
385 perturbation and assisted towing methods, was substantially less than our study at 1.59  
386 (Havriluk, 2007). Differences in drag coefficients may be due to the assumption used in  
387 active drag methodologies, that a swimmer's velocity remains constant throughout the  
388 stroke cycle, rather than fluctuating. In studies that have determined drag coefficients

389 during underwater gliding using deceleration force of swimmers, drag coefficients were  
390 also calculated using a mean value of deceleration and velocity throughout the glide  
391 (Morais et al., 2013; Vilas-Boas et al., 2010). In contrast, the current study derived drag  
392 coefficients at the instant of maximum horizontal deceleration rather than a mean value  
393 representing the entire stroke cycle, which may explain the differences in drag  
394 coefficients between studies. Added and/or subtracted active drag methods may alter  
395 regular swimming technique as the swimmers are physically attached to a pulley system  
396 or towing a hydrodynamic buoy, manipulating the stimulus they are regularly exposed to.  
397 Swimmers in the current study performed front crawl swimming without changes to their  
398 regular swimming technique highlighting the utility of deriving an instantaneous  
399 maximum drag coefficient from the deceleration phase of the stroke cycle when assessing  
400 the influence of human morphology on the coefficient of drag.

401 Findings from the current study have implications for talent identification for  
402 middle-long distance front crawl swimming, where swimmers with optimal torso shapes  
403 may exhibit greater swimming efficiency than swimmers with greater body shape  
404 variability from waist-hip. A focus on improving swimming efficiency and optimising  
405 the hydrodynamic body position appears to be the most advantageous approach to  
406 improving swimming performance (Morais et al., 2012). Manipulation of front crawl  
407 technique to minimise excessive lordosis through the lumbar spine may reduce the  
408 posterior form gradient from waist-hip and subsequent fluid flow deviation. For example,  
409 feedback and cuing of swimmers to actively engage gluteal muscles during front crawl  
410 may assist in maintaining neutral pelvic alignment and minimise hip curvature.  
411 Improvements in hydrodynamic resistance have been achieved previously by providing  
412 feedback and cuing to manipulate swimmers' posture during underwater gliding (Thow,  
413 Naemi, & Sanders, 2012) .

414 Manipulation of torso morphology has been evident in the design of competitive  
415 swimsuits. While the Swimwear Approval Committee of FINA assesses competitive  
416 swimsuits with specific guidelines on the material makeup and characteristics of the  
417 swimsuit (e.g. thickness, buoyancy and permeability), investigating the effect of new  
418 swimsuits on body curvatures and the subsequent hydrodynamic resistance ought to be  
419 considered, especially for female swimsuits that cover the chest, waist and hips. Other  
420 than using swimsuits, body sculpting through training and nutritional strategies may be  
421 implemented to improve hydrodynamic shape. However, researchers carrying out this  
422 approach would need to consider how changes in body shape may alter the power to  
423 weight ratio of the swimmer. Further investigations involving male and female swimmers  
424 would be advantageous to investigate whether differences in body shape exist between  
425 sexes and the potential influence that different body contours and curvatures have on  
426 hydrodynamic resistance.

427 The current study has several limitations that ought to be considered when  
428 interpreting the findings. Body shape influences the mass of fluid moving in conjunction  
429 with the body (Caspersen et al., 2010), thereby affecting inertia and the magnitude of  
430 deceleration (Naemi & Sanders, 2008). While maximum deceleration of the body was  
431 used to calculate the drag coefficient in our study, the maximum instantaneous force was  
432 based partly on an estimate of added mass rather than a known value. As a consequence,  
433 the effect of torso shape on added mass and the drag coefficient could not be measured  
434 directly. Waist-hip morphology during the static standing body position is comparable to  
435 the body position during the non-propulsive hand phase of front crawl swimming.  
436 Morphological differences, however, may occur between the static standing and non-  
437 propulsive hand phase body positions, as the chest-waist segment may be manipulated  
438 when the arms are outstretched above the head. Deriving torso curvatures and

439 indentations from underwater images of the swimmer at key instances throughout the  
440 stroke cycle in future research would be advantageous to further our understanding of the  
441 hydrodynamic profile of human swimmers. Furthermore, results from the bootstrapping  
442 statistical method revealed that the 95% confidence intervals of Pearson correlation  
443 coefficients ranged from ‘weak’ to ‘strong’ for both predictors of the drag coefficient;  
444 rate of change in CSA waist-hip and posterior form gradient waist-hip. Further research  
445 involving larger sample sizes would be advantageous to improve the accuracy of the  
446 relationship magnitude between waist-hip morphology and the drag coefficient.

#### 447 **Conclusions**

448 Preliminary findings have shown that a significant relationship exists between the rate of  
449 change in shape from the waist to the hip and the coefficient of drag. Greater indentation  
450 at the waist and ‘bulge’ of the buttocks may result in deviation to fluid flow and  
451 turbulence in the lumbar region of the swimmer’s posterior aspect that result in increased  
452 hydrodynamic resistance. The method of quantifying torso shape described in this paper  
453 will be applied in further investigations to determine the influence of torso curvatures and  
454 shape, of male and female swimmers, on glide efficiency, to develop an understanding of  
455 how performance in the underwater glide phase of swimming can be improved.

#### 456 **Acknowledgements**

457 We would like to thank Professors Joao Paulo Vilas-Boas and Ricardo Fernandes and  
458 their research team at the University of Porto, Portugal, for their contributions in  
459 recruiting swimmers and facilitating data collection at that venue.

460 **References**

- 461 Alcock, A., & Mason, B. (2007). Biomechanical analysis of active drag in swimming.  
462 *Proceedings of XXV International Symposium on Biomechanics in Sports*, Ouro  
463 Preto, Brazil, 212-215.
- 464 Beaumont, F., Taïar, R., & Polidori, G. (2017). Preliminary numerical investigation in  
465 open currents-water swimming: Pressure field in the swimmer wake. *Applied*  
466 *Mathematics and Computation*, 302, 48-57.
- 467 Benjanuvatra, N., Blanksby, B. A., & Elliott, B. C. (2001). Morphology and  
468 hydrodynamic resistance in young swimmers. *Pediatric Exercise Science*, 13(3),  
469 246-255.
- 470 Caspersen, C., Berthelsen, P. A., Eik, M., Pâkozdi, C., & Kjendlie, P-L. (2010). Added  
471 mass in human swimmers: age and gender differences. *Journal of Biomechanics*,  
472 43(12), 2369-2373.
- 473 Deffeyes, J., & Sanders, R. (2005). Elliptical zone body segment modelling software:  
474 digitising, modelling and body segment parameter calculation. *Proceedings of*  
475 *XXIII International Symposium on Biomechanics in Sports*, Beijing, China, 749-  
476 752.
- 477 Evans, J. D. (1996). *Straightforward statistics for the behavioral sciences*. Pacific Grove:  
478 Thomson Brooks/Cole Publishing Co.
- 479 Fish, F. E., & Hui, C. A. (1991). Dolphin swimming—a review. *Mammal Review*, 21(4),  
480 181-195.
- 481 Gatta, G., Cortesi, M., Fantozzi, S., & Zamparo, P. (2015). Planimetric frontal area in the  
482 four swimming strokes: Implications for drag, energetics and speed. *Human*  
483 *movement science*, 39, 41-54.
- 484 Gonjo, T., McCabe, C., Coleman, S., Soares, S., Fernandes, R. J., Vilas-Boas, J. P., &  
485 Sanders, R. (2019). Do swimmers conform to criterion speed during pace-

486 controlled swimming in a 25-m pool using a visual light pacer? *Sports*  
487 *biomechanics*, 1-14.

488 Havriluk, R. (2005). Performance level differences in swimming: a meta-analysis of  
489 passive drag force. *Research quarterly for exercise and sport*, 76(2), 112-118.

490 Havriluk, R. (2007). Variability in measurement of swimming forces: a meta-analysis of  
491 passive and active drag. *Research quarterly for exercise and sport*, 78(2), 32-39.

492 Hertel, H. (1966). *Structure, form, movement*. New York: Reinhold.

493 Hollander, A., De Groot, G., van Ingen Schenau, G., Toussaint, H., De Best, H., Peeters,  
494 W., . . . Schreurs, A. (1986). Measurement of active drag during crawl arm stroke  
495 swimming. *Journal of sports sciences*, 4(1), 21-30.

496 Huijing, P., Toussaint, H., Mackay, R., Vervoorn, K., Clarys, J., & Hollander, A. (1988).  
497 Active drag related to body dimensions. *Swimming science V*, 18, 31-37.

498 Jensen, R. K. (1978). Estimation of the biomechanical properties of three body types  
499 using a photogrammetric method. *Journal of biomechanics*, 11(8-9), 349-358.

500 Juan, S., & Lantz, F. (2001). Application of bootstrap techniques in econometrics: the  
501 example of cost estimation in the automotive industry. *Oil & Gas Science and*  
502 *Technology*, 56(4), 373-388.

503 Lyttle, A. D., Blanksby, B., Elliot, B., & Lloyd, D. G. (1998). The effect of depth and  
504 velocity on drag during the streamlined guide. *Journal of Swimming Research*,  
505 13, 15-22.

506 Machtsiras, G. (2012). *Utilizing flow characteristics to increase performance in*  
507 *swimming*. (Doctor of Philosophy), The University of Edinburgh, Edinburgh,  
508 Scotland.

509 MacKinnon, D. P., Lockwood, C. M., & Williams, J. (2004). Confidence limits for the  
510 indirect effect: Distribution of the product and resampling methods. *Multivariate*  
511 *behavioral research*, 39(1), 99-128.

512 Marinho, D., Barbosa, T., Rouboa, A., & Silva, A. (2011). The hydrodynamic study of  
513 the swimming gliding: a two-dimensional computational fluid dynamics (CFD)  
514 analysis. *Journal of Human Kinetics*, 29, 49-57.

515 McCabe, C. B., & Sanders, R. H. (2012). Kinematic differences between front crawl  
516 sprint and distance swimmers at a distance pace. *Journal of sports sciences*, 30(6),  
517 601-608.

518 Mollendorf, J. C., Albert, T., C, Oppenheim, E., & Pendergast, D. R. (2004). Effect of  
519 swim suit design on passive drag. *Medicine & Science in Sports & Exercise*, 36(6),  
520 1029-1035.

521 Morais, J. E., Costa, M., Mejias, E., Marinho, D., Silva, A., & Barbosa, T. (2011).  
522 Morphometric study for estimation and validation of trunk transverse surface area  
523 to assess human drag force on water. *Journal of Human Kinetics*, 28, 5-13.

524 Morais, J. E., Jesus, S., Lopes, V., Garrido, N., Silva, A., Marinho, D., & Barbosa, T. M.  
525 (2012). Linking selected kinematic, anthropometric and hydrodynamic variables  
526 to young swimmer performance. *Pediatric Exercise Science*, 24(4), 649-664.

527 Morais, J. E., Jesus, S., Mejias, J. E., Costa, M. J., Moreira, M., Garrido, N. D., . . .  
528 Barbosa, T. M. (2013). Is the underwater gliding test a valid procedure to estimate  
529 the swimmers' drag? *International SportMed Journal*, 14(4), 216-225.

530 Naemi, R., & Sanders, R. H. (2008). A “hydrokinematic” method of measuring the glide  
531 efficiency of a human swimmer. *Journal of biomechanical engineering*, 130(6).

532 Nicolas, G., Bideau, B., Colobert, B., & Berton, E. (2007). How are Strouhal number,  
533 drag, and efficiency adjusted in high level underwater monofin-swimming?  
534 *Human movement science*, 26(3), 426-442.

535 Papic, C., McCabe, C., Naemi, R., & Sanders, R. (2019). A method of quantifying torso  
536 shape to assess its influence on resistive drag in swimming. *ISBS Proceedings*  
537 *Archive*, 37(1), 113.

538 Pease, D., & Vennell, R. (2011). Comparison of wave drag for both the male and female  
539 form. *Proceedings of XXIX International Society of Biomechanics in Sports*,  
540 Porto, Portugal, 355-358.

541 Pendergast, D., Mollendorf, J., Zamparo, P., Termin 2nd, A., Bushnell, D., & Paschke,  
542 D. (2005). The influence of drag on human locomotion in water. *Undersea and*  
543 *Hyperbaric Medical Society*, 32(1), 45-57.

544 Psycharakis, S., Naemi, R., Connaboy, C., McCabe, C., & Sanders, R. (2010). Three-  
545 dimensional analysis of intracycle velocity fluctuations in frontcrawl swimming.  
546 *Scandinavian Journal of Medicine & Science in Sports*, 20(1), 128-135.

547 Seifert, L., Chollet, D., & Bardy, B. (2004). Effect of swimming velocity on arm  
548 coordination in the front crawl: a dynamic analysis. *Journal of sports sciences*,  
549 22(7), 651-660.

550 Thow, J. L., Naemi, R., & Sanders, R. H. (2012). Comparison of modes of feedback on  
551 glide performance in swimming. *Journal of sports sciences*, 30(1), 43-52.

552 Toussaint, H., De Groot, G., Savelberg, H., Vervoorn, K., Hollander, A., & van Ingen  
553 Schenau, G. (1988). Active drag related to velocity in male and female swimmers.  
554 *Journal of biomechanics*, 21(5), 435-438.



555 Van der Vaart, A., Savelberg, H., De Groot, G., Hollander, A., Toussaint, H., & van Ingen  
556 Schenau, G. (1987). An estimation of drag in front crawl swimming. *Journal of*  
557 *biomechanics*, 20(5), 543-546.

558 Vilas-Boas, J. P., Costa, L., Fernandes, R. J., Ribeiro, J., Figueiredo, P., Marinho, D., . .  
559 . Machado, L. (2010). Determination of the drag coefficient during the first and  
560 second gliding positions of the breaststroke underwater stroke. *Journal of Applied*  
561 *Biomechanics*, 26(3), 324-331.

562 Zamparo, P., Gatta, G., Pendergast, D., & Capelli, C. (2009). Active and passive drag:  
563 the role of trunk incline. *European journal of applied physiology*, 106(2), 195-  
564 205.

565

566 **Tables**

567 Table 1. Mean (standard deviation) torso shape and drag coefficient measurements for  
 568 Group 1, Group 2 and Combined Cohort.

<b>Outcome measure</b>	<b>Group 1 (n = 15)</b>	<b>Group 2 (n = 10)</b>	<b><i>p</i></b>	<b>Combined (n = 25)</b>
Body mass (kg)	73.90 (8.73)	70.04 (6.63)	0.223	72.36 (8.04)
Torso length (m)	0.649 (0.026)	0.656 (0.030)	0.579	0.652 (0.988)
Cross sectional area (m <sup>2</sup> )				
Chest	0.070 (0.009)	0.067 (0.007)	0.394	0.069 (0.008)
Waist	0.045 (0.005)	0.047 (0.006)	0.556	0.046 (0.005)
Hip	0.065 (0.006)	0.066 (0.007)	0.865	0.065 (0.006)
Rate of change in CSA (m <sup>2</sup> /m)				
Chest-waist	-0.178 (0.046)	-0.171 (0.035)	0.694	-0.175 (0.413)
Waist-hip	0.214 (0.032)	0.204 (0.051)	0.591	0.210 (0.040)
Form gradients (m/m)				
Anterior chest-waist	-0.197 (0.109)	-0.220 (0.137)	0.662	-0.206 (0.119)
Anterior waist-hip	0.281 (0.149)	0.323 (0.105)	0.416	0.298 (0.132)
Posterior chest-waist	-0.337 (0.082)	-0.348 (0.150)	0.848	-0.341 (0.112)
Posterior waist-hip	0.597 (0.153)	0.504 (0.152)	0.152	0.560 (0.157)
Lateral (left) chest-waist	-0.298 (0.107)	-0.303 (0.080)	0.902	-0.300 (0.095)
Lateral (left) waist-hip	0.318 (0.070)	0.257 (0.072)	0.050	0.294 (0.076)
Lateral (right) chest-waist	-0.299 (0.071)	-0.294 (0.088)	0.883	-0.297 (0.077)
Lateral (right) waist-hip	0.250 (0.079)	0.277 (0.089)	0.453	0.260 (0.082)
Drag coefficient	3.18 (1.07)	2.62 (0.74)	0.133	2.96 (0.98)

569

570 Table 2. Pearson correlation coefficient between torso shape measurements and the drag  
 571 coefficient (n=25).

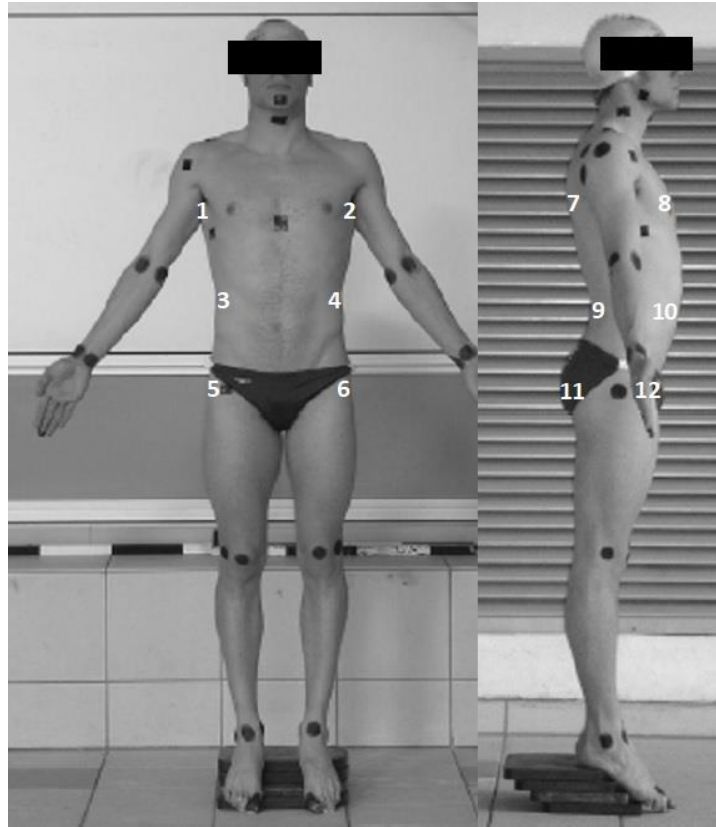
<b>Torso shape measurements</b>	<b><i>r</i></b>	<b><i>p</i></b>
Torso length (m)	-0.19	0.177
Body mass (kg)	-0.03	0.438
Cross sectional areas (m <sup>2</sup> )		
Chest	0.01	0.475
Waist	0.23	0.134
Hip	0.16	0.222
Rate of change in cross-sectional area (m <sup>2</sup> /m)		
Chest-waist	0.18	0.192
Waist-hip	0.44*	0.014
Form gradients (m/m)		
Anterior chest-waist	0.09	0.335
Anterior waist-hip	0.08	0.346
Posterior chest-waist	-0.16	0.217
Posterior waist-hip	0.50**	0.006
Lateral (left) chest-waist	0.23	0.132
Lateral (left) waist-hip	0.18	0.195
Lateral (right) chest-waist	0.32	0.060
Lateral (right) waist-hip	-0.16	0.224

572 \*  $p < 0.05$ , \*\* $p < 0.01$

573

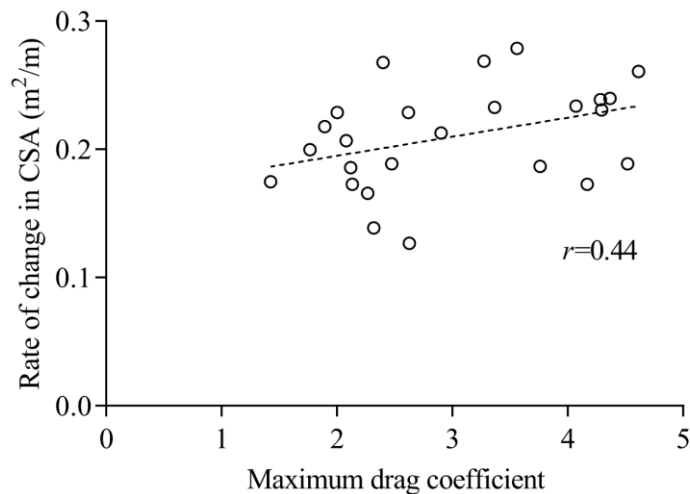
574 **Figure captions**

575 Figure 1. Maximum segment form gradient (m/m): Lateral (right) chest-waist (1–3) and  
576 waist-hip (3–5), lateral (left) chest-waist (2–4) and waist-hip (4–6), posterior chest-waist  
577 (7–9) and waist-hip (9–11), anterior chest-waist (8–10) and waist-hip (10–12).



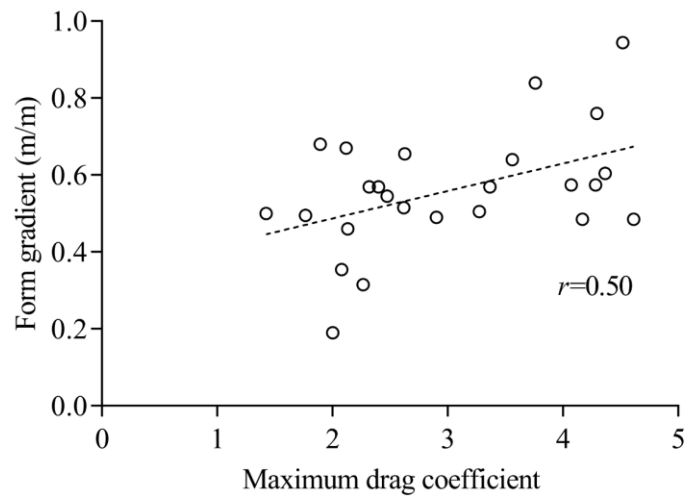
578

579 Figure 2. Maximum rate of change in cross sectional area waist-hip vs maximum drag  
580 coefficient.



581

582 Figure 3. Maximum posterior form gradient waist-hip vs maximum drag coefficient.



583